

## X-ray-diffraction spectra of deterministic nonperiodic structures: Dynamical versus kinematical theory

G. C. La Rocca

*Scuola Normale Superiore, 56100 Pisa, Italy  
and Max-Planck-Institut fuer Festkoerperforschung, 7000 Stuttgart 80, Germany*

L. Tapfer

*Centro Nazionale Ricerca e Sviluppo Materiali, 72023 Mesagne (Br), Italy  
and Max-Planck-Institut fuer Festkoerperforschung, 7000 Stuttgart 80, Germany*

R. Cingolani

*Dipartimento Scienza dei Materiali, Università di Lecce, 73100 Lecce, Italy  
and Max-Planck-Institut fuer Festkoerperforschung, 7000 Stuttgart 80, Germany*

K. Ploog

*Max-Planck-Institut fuer Festkoerperforschung, 7000 Stuttgart 80, Germany  
(Received 11 December 1991)*

Layered systems (e.g., semiconductor superlattices) with a deterministic nonperiodic structure exhibit characteristic lengths at all scales, therefore their properties are especially interesting in the infinite limit. X-ray-diffraction spectra of such systems are usually analyzed in terms of their Fourier transforms, i.e., within the kinematical theory of scattering. The diffraction pattern of an infinite lattice, though, is rigorously described only by the dynamical theory of scattering which, in particular, takes multiple reflections and extinction into account. As an example, the diffraction pattern of the Thue-Morse lattice is studied theoretically in the infinite limit. The results of high-resolution x-ray diffraction measurements on a GaAs-AlAs Thue-Morse superlattice are presented and analyzed. Photoluminescence and photoluminescence excitation spectra of the same structure are also discussed.

### I. INTRODUCTION

Since the discovery of quasicrystals, considerable attention has been paid to nonperiodic, yet deterministically ordered structures, both theoretically and experimentally. Much studied have been the one-dimensional realizations of such systems in the form of semiconductor superlattices, either quasiperiodic (e.g., the Fibonacci lattice) or more general (e.g., the Thue-Morse lattice). Their x-ray-diffraction spectra, in particular, clearly show characteristic features of the nonperiodic order.<sup>1</sup> Such diffraction patterns are related to the Fourier transform of the underlying structures, which have been theoretically studied also in the infinite limit.<sup>2</sup> For a thick system, though, the effects of extinction and multiple reflections cannot be neglected and a weak-scattering theory such as the kinematical theory is, in principle, inadequate. In particular, the x-ray-diffraction pattern of a thick superlattice is not simply related to the Fourier transform of its compositional profile, but can be correctly described only by the dynamical theory of scattering.<sup>3</sup> In Sec. II the diffraction pattern of a model of the infinite Thue-Morse lattice is theoretically studied within the dynamical theory. In Sec. III high-resolution x-ray-diffraction spectra of a GaAs-AlAs Thue-Morse superlattice are presented and discussed, along with the results of optical measurements on the same structure. In the experiments,

even if the diffraction pattern clearly reveals the underlying nonperiodic order, the total thickness is not enough for the kinematical theory to break down. In this sense the available samples (see also Ref. 1) are far from the infinite limit investigated in Sec. II.

### II. THEORY (INFINITE LIMIT)

Using two building blocks  $A$  and  $B$ , the Thue-Morse lattice ( $ABBAABAAB\cdots$ ) can be defined recursively as indicated in Fig. 1(a) with the  $g$ th-generation approximant containing  $2^g$  elementary blocks ( $A$  and  $B$ ).<sup>1,4</sup> To calculate its diffraction pattern within the dynamical theory,<sup>5</sup> it is convenient to set up a system of recursion relations for the reflection and transmission amplitudes of successive generation approximants. Referring to Fig. 1(b),  $r$ ,  $\bar{r}$ ,  $t$ , and  $\bar{t}$  for the  $(g+1)$ th approximant are given in terms of the same quantities for the  $g$ th approximant as follows:

$$\begin{aligned} r_{g+1} &= r_g + t_g r_{\bar{g}} \bar{t}_g + t_g r_{\bar{g}} \bar{r}_g r_{\bar{g}} \bar{t}_g + \cdots \\ &= r_g + t_g r_{\bar{g}} \frac{1}{1 - \bar{r}_g r_{\bar{g}}} \bar{t}_g, \end{aligned} \quad (1a)$$

$$\begin{aligned} t_{g+1} &= t_g \bar{t}_g + t_g r_{\bar{g}} \bar{r}_g \bar{t}_g + \cdots \\ &= t_g \frac{1}{1 - \bar{r}_g r_{\bar{g}}} \bar{t}_g, \end{aligned} \quad (1b)$$

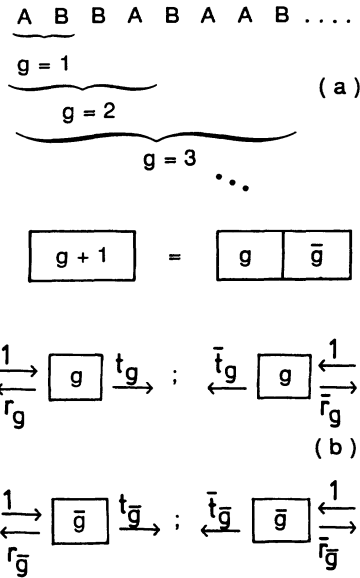


FIG. 1. (a) Generation rule of the Thue-Morse lattice ( $\overline{A} = B$ ,  $\overline{B} = A$ ,  $\overline{AB} = \overline{A}\overline{B} = BA$ , etc.). (b) Definition of reflection and transmission amplitudes, from the left and from the right (in all cases,  $r^*r + t^*t = 1$ ).

and similar equations for  $\bar{t}_{g+1}$  and  $\bar{r}_{g+1}$ . The reflection and transmission amplitudes for a single homogeneous slab ( $A$  or  $B$ ) are written in general as<sup>6</sup>

$$r_{A,B} = i\rho_{A,B} e^{i\varphi_{A,B}},$$

$$t_{A,B} = (1 - \rho_{A,B}^2)^{1/2} e^{i\varphi_{A,B}},$$

with

$$-1 \leq \rho_{A,B} \leq 1.$$

The Thue-Morse lattice is modeled as simply as possible setting  $\Phi_A = \Phi_B = \Phi_0$  and  $\rho_A = -\rho_B = \rho_0$ ; then, using the generation rule, it follows that

$$t_g = t_{\bar{g}} = \bar{t}_g, \tag{2a}$$

$$r_g = -r_{\bar{g}} = (-1)^g \bar{r}_g, \tag{2b}$$

and

$$r_g^2 = (-1)^{g+1} t_g^2 \left[ \frac{1 - t_g^* t_g}{t_g^* t_g} \right] \tag{2c}$$

Finally, from Eqs. (1) and (2), the following recursion relation<sup>7</sup> for the quantity  $q_g = 1/t_g$  is derived:

$$q_{g+1} = 1 + q_g^2 - q_g^* q_g, \tag{3}$$

with

$$q_0 = \frac{1}{t_A} = \frac{e^{-i\varphi_0}}{(1 - \rho_0^2)^{1/2}}.$$

Thus, within the dynamical theory, the diffraction pat-

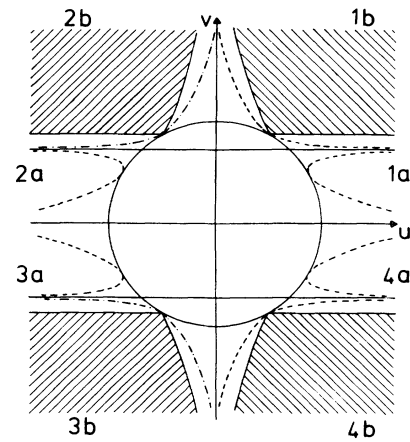


FIG. 2. Domain  $D$  ( $|uv| > \sqrt{3}/4$  and  $|v| > \sqrt{3}/2$ ) is comprised of the shaded regions; the boundary of the invariant manifolds is sketched by the dot-dashed lines, with a few preimages sketched by the dashed lines (see text for details).

tern of this model of the Thue-Morse lattice is given in the infinite limit by

$$R_\infty(\rho_0, \varphi_0) = \lim_{g \rightarrow \infty} (r_g^* r_g) = \lim_{g \rightarrow \infty} \left[ 1 - \frac{1}{q_g^* q_g} \right],$$

where it is convenient to fix  $\rho_0$  between 0 and 1 and vary  $\Phi_0$  (without loss of generality  $\Phi_0$  can be restricted to the range  $[0, \pi/2]$ ).

With reference to Fig. 2 and considering only the region outside the unit circle ( $q = u + iv$ ,  $q^*q > 1$ ) under the continuous mapping of Eq. (3) the first quadrant goes into

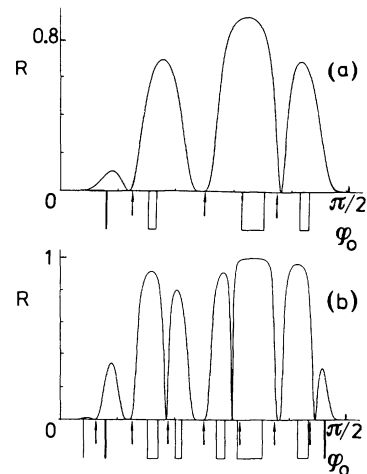


FIG. 3. Reflectivity pattern of the Thue-Morse lattice according to the mapping of Eq. (3) as a function of  $\Phi_0$  with  $\rho_0 = 0.2$ . Shown above the horizontal axis are (a) the fourth- and (b) the fifth-generation spectra; the vertical rectangles below the axis mark the ranges corresponding to points mapped into the domain  $D$  after (a) two and (b) three iterations. Also marked by arrows are the reflectivity zeros predicted by the kinematical theory.

the first and second ones, the second one into the third and fourth ones, the third one into the first and second ones, and the fourth one into the third and fourth ones; in particular, the region 1a below the line  $v=1/\sqrt{2}$  goes into the first quadrant and the region 1b above the same line into the second one, and similarly for the other regions shown in Fig. 2. The points with  $u=0$  and  $|v|>1$  go into points with  $v=0$  and  $u<-1$  and the latter go into the fixed point ( $u=1, v=0$ ), which corresponds to vanishing reflectivity (i.e., perfect transmission). This is the only way in which, starting with  $\rho_0>0$  ( $\Phi_0>0$ ), a vanishing reflectivity can be achieved, and for  $\Phi_0$  varying from 0 to  $2\pi$ ,  $2^g$  reflectivity zeros are obtained after the  $g$ th iteration of the mapping ( $g>0$ ), which gives the diffraction pattern of the  $g$ th-generation approximant within the dynamical theory. These zeros do not have a simple analytical expression,<sup>8</sup> whereas the kinematical theory would give reflectivity zeros for the  $g$ th generation simply at  $\Phi(g, n)=2\pi n/2^g$ , with  $n=0, 1, \dots, (2^g-1)$  (cf. Figs. 3 and 4). With regard to x-ray diffraction, more significant than the reflectivity zeros are the ranges of  $\Phi_0$  for which a large reflectivity is obtained, in particular those ranges which correspond, in the infinite limit, to total reflectivity ( $R_\infty=1$ ). In this instance the kinematical theory is definitely inadequate and the scaling of the peak intensity with the generation number predicted on the basis of the Fourier transform of the compositional profile breaks down as soon as the reflectivity becomes comparable to unity. The mapping of Eq. (3) admits an invariant manifold consisting of only two regions transforming into one another (one in the second and one in the third quadrant). As sketched in Fig. 2, the boundary of the first one is tangent to the unit circle at the point ( $u=-\frac{1}{2}, v=\sqrt{3}/2$ ) and approaches asymptotically the lines  $v=1/\sqrt{2}$  and  $u=0$  (the second region is obtained from the first changing the sign of  $v$ ). The points in the interior of this domain and of all its preimages of which those of order one and two are sketched in Fig. 2, respectively, within region 1b (or 4b) and regions 1a and 3a (or 4a and 2a), escape to infinity, which means that they give

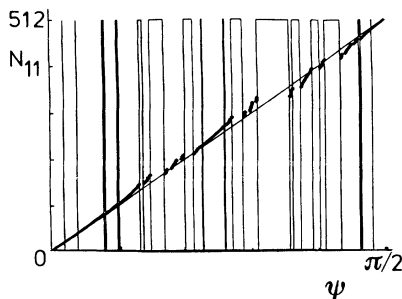


FIG. 4. Total number  $N_{11}(\Psi)$  of reflectivity zeros, according to the mapping of Eq. (3), with  $\Phi_0$  between 0 and  $\Psi$  for the 11th-generation approximant with  $\rho_0=0.2$ . The kinematical theory would simply give for  $N_{11}(\Psi)$  the integer part of  $(2^{11}\Psi/2\pi)$  as indicated by the solid line; note, instead, the wide ranges of  $\Phi_0$  where zeros are absent and how they mostly correspond to points mapped into the domain  $D$  already after only four iterations, as marked by the vertical rectangles.

rise to total reflectivity. As a closed expression for the boundary of the invariant manifold described above could not be found, in order to show how in the infinite limit there are ranges of  $\Phi_0$  of finite extension giving rise to total reflectivity, the domain  $D$  defined for analytical convenience by  $|uv|>\sqrt{3}/4$  and  $|v|>\sqrt{3}/2$  (shown by the shaded areas in Fig. 2) is studied in the following. Under the mapping of Eq. (3), once a point is taken inside  $D$ , it stays in  $D$ ; furthermore, if  $q_M$  belongs to  $D$ , it follows that, for all  $n>M-1$ ,

$$\begin{aligned} |q_{n+1}|^2 &= 1 + 4v_n^2(|q_n|^2 - 1) \\ &> 1 + 3(|q_n|^2 - 1) > |q_n|^2 \end{aligned}$$

and also

$$\frac{|q_{n+1}|^2}{|q_n|^2} > 3 - \frac{2}{|q_n|^2} > 3 - \frac{2}{|q_M|^2} > 1,$$

which implies

$$\lim_{n \rightarrow \infty} |q_n|^2 = \infty;$$

i.e., once a point is mapped into  $D$ , it escapes to infinity. As a consequence, the extended ranges of  $\Phi_0$  that, at a given iteration  $M$ , correspond to points within  $D$  give rise, in the infinite limit, to total reflectivity regions, as pictured in Fig. 3 [see, in particular, the range  $\Phi_0/\pi \sim 0.33$  in Fig. 3(b)]. Moreover, within these intervals of  $\Phi_0$ , no reflectivity zeros can ever be obtained, in contrast to the predictions of the kinematical theory discussed above (cf. Fig. 3 and, especially, Fig. 4).

### III. EXPERIMENT (FINITE SIZE)

A semiconductor superlattice fabricated according to the Thue-Morse generation rule using a layer of GaAs as the  $A$  building block and one of AlAs as the  $B$  building block [cf. Fig. 1(a)] has been investigated by high-resolution x-ray diffraction and by photoluminescence and photoluminescence excitation spectroscopy. Figure 5(a) shows the diffraction pattern of the eight-generation approximant (256 layers) in proximity of the (200) reflection. As shown in Fig. 5(b), employing literature values for the parameters of the bulk materials,<sup>9</sup> a very satisfactory fit is obtained with a GaAs layer thickness of 4.1 nm and an AlAs layer thickness of 2.5 nm (in close agreement with estimates based on growth rates). In the simulation a constant background at the level of  $10^{-4}$  and a broadening of  $10^{-4}$  rad are included. As evident from Fig. 5, the superlattice quality is excellent and all the side peaks predicted above the background as a consequence of the Thue-Morse nonperiodic order are resolved. However, the corresponding reflectivity values are only of the order of  $10^{-3}$ ; therefore the diffraction pattern shown here is far from the infinite limit discussed above, as a result of limitations in the total thickness of the sample.

Figure 6 shows the photoluminescence (PL) and photoluminescence excitation (PLE) spectra of the same sample. Structures related to the nonperiodic order of the superlattice are not clearly recognizable. Actually, the

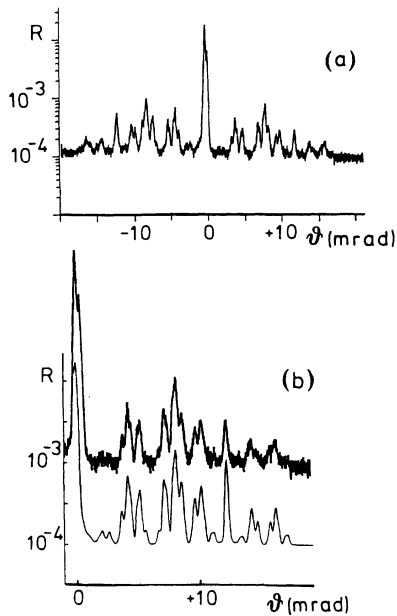


FIG. 5. (a) High-resolution x-ray-diffraction pattern of the eighth-generation Thue-Morse lattice near the (200) reflection; (b) fit to the data shown in (a), the experimental curve has been vertically shifted by a decade for clarity (see text for details).

spectra can be roughly interpreted on the basis of the simultaneous presence of single wells (i.e., isolated  $A$  blocks sandwiched by  $B$  blocks) and of double wells (i.e., two contiguous  $A$  blocks sandwiched by  $B$  blocks) as a consequence of the Thue-Morse generation rule [see Fig. 1(a)]. In particular, the two low-energy PLE peaks at

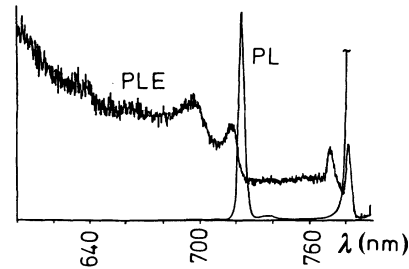


FIG. 6. Photoluminescence excitation (PLE) and photoluminescence (PL) spectra of the eighth-generation Thue-Morse lattice. The vertical scale is linear for both PLE and PL, in arbitrary units. The main luminescence peak (extending from about 780 to about 800 nm) is truncated as it is about two orders of magnitude stronger than the peak at 723 nm.

about 780 nm correspond to the first heavy-hole and first light-hole transitions in the double wells, the next peak at 717 nm falls between the first heavy-hole and first light-hole transitions in the single wells, and the broader one at 688 nm corresponds to the second heavy-hole transition in the double wells (the second light-hole transition in the double wells is calculated at about 665 nm, where no resolved structure is evident). As for the PL spectrum, besides the main peak of the first heavy-hole transition in the double wells (corresponding to the lowest-lying electronic excitation), an additional peak, about two orders of magnitude weaker, is clearly observed at 723 nm in correspondence of the first heavy-hole transition in the single wells, indicating that not all carriers excited in the narrow wells are collected in the large ones before they recombine.

<sup>1</sup>L. Tapfer, Phys. Scr. T **25**, 45 (1989); F. Axel and H. Terauchi, Phys. Rev. Lett. **66**, 2223 (1991), and references therein.

<sup>2</sup>C. Godreche and J. M. Luck, J. Phys. A **23**, 3769 (1990), and references therein.

<sup>3</sup>See, for instance, W. H. Zachariasen, *Theory of X-ray Diffraction in Crystals* (Dover, New York, 1967).

<sup>4</sup>Z. Cheng, R. Savit, and R. Merlin, Phys. Rev. B **37**, 4375 (1988).

<sup>5</sup>See, for periodic superlattices, D. M. Vardanyan, H. M. Manoukian, and H. M. Petrosyan, Acta Crystallogr. A **41**, 212 (1985).

<sup>6</sup> $\rho$  is related to the structure factor and  $\Phi$  to the deviation from the Bragg condition; see Refs. 3 and 5.

<sup>7</sup>Note that, because of the presence of the term  $q^*q$  in Eq. (3), the extensive mathematical literature about the iterates of holomorphic functions is not directly applicable.

<sup>8</sup>For the conditions giving rise to perfect transmission of light through nonperiodic dielectric superlattices, see M. Kohmoto, B. Sutherland, and K. Iguchi, Phys. Rev. Lett. **58**, 2436 (1987) and M. Kolar, M. K. Ali, and F. Nori, Phys. Rev. B **43**, 1034 (1991).

<sup>9</sup>L. Tapfer and K. Ploog, Phys. Rev. B **33**, 5565 (1986).